2021

Modeling and Analysis of Pressure Drop Oscillations in Horizontal Boiling Flow

Hongtao Qiao
Mitsubishi Electric Research Laboratories, United States of America, qiao@merl.com

Christopher Laughman

Modeling and Analysis of Pressure Drop Oscillations in Horizontal Boiling Flow

Hongtao QIAO*, Christopher R. LAUGHMAN

Mitsubishi Electric Research Laboratories
Cambridge, MA 02139, USA
{qiao, laughman}@merl.com

ABSTRACT

In general, two-phase flow phenomena can be described based on the one-dimensional conservation laws. Models with different formulations can be obtained with different assumptions. This paper presents three models with different complexity to simulate pressure drop oscillations. The direct comparison indicates that there are substantial differences between these models. The mechanism of pressure drop oscillations is discussed and the effect of operating parameters on system instability is explored. It is shown that two bifurcation points can exist when varying heat input and inlet subcooling. Root locus analysis corroborates the simulation results.

Keywords: Thermo-hydraulic, Instabilities, Two-phase, Boiling flow, Pressure drop oscillations, Modeling

1. INTRODUCTION

Two-phase flow boiling systems are widely used in the HVAC&R, power generation, thermal management, chemical and other industries. Under certain conditions the pressure-drop vs. flow-rate characteristic curve of a boiling system (internal curve) may exhibit an N-shape (or S-shape) due to distinct thermal-hydraulic behavior between liquid, two-phase and vapor. Depending on the corresponding characteristic curve of the external system, the operational points can be stable or unstable. When system operation is unstable, repeated oscillations of flow rate and system pressure occur and can cause undesirable issues such as mechanical vibrations, thermal fatigue and control failure. Under extreme circumstances, flow oscillations are so severe that the amount of fluid flow in the system may decrease dramatically, leading to elevated heat transfer surface temperatures and possible system burnout (Ruspini et al., 2014).

Thermally induced flow instabilities are of a great concern in the design and operation of many industry systems and thus have drawn attention of many researchers. A whole series of interesting and noteworthy papers focusing on experimental investigations and theoretical analyses on dynamic instabilities of two-phase flow have been published since 1960s. In general, two-phase dynamic instabilities can be classified into the following categories based on different physical mechanisms, Ledinegg instability, pressure-drop oscillations (PDO) and density-wave oscillations (DWO), etc. Ledinegg instability often occurs when the slope of the internal characteristic curve is negative and steeper than the external characteristic curve and multiple intersections of the internal and external characteristics exist. Different from Ledinegg instability, the conditions for the occurrence of PDO require the external characteristics steeper than the internal characteristics and the presence of a compressible volume in the flow circuit. In comparison with low-frequency PDO, high-frequency DWO is caused by the delay in the propagation of disturbances and the feedback processes conditioning the inlet parameters. Due to page limit constraints, we are unable to discuss in detail all three types of flow instabilities. This presented paper will focus on the mathematical modeling and analysis of PDO.

Two-phase flow phenomena can be described based on the one-dimensional conservation laws. Models with different formulations can be obtained with different assumptions. Among the models that are used to predict the flow instabilities, the integral method is often applied to model the heater tube of the involved system because it can significantly reduce the dimensionality of the problem. With this method, the dynamic behavior of fluid in the heater tube is neglected and steady-state equilibrium conditions with linear enthalpy profile are assumed even during transients. Although this simplified model provides insight when conducting stability analysis, its underlying assumptions cannot be fulfilled under certain conditions, resulting in completely opposite predictions when comparing with other models. Another popular choice is to use high-order fully discretized formulation based on finite difference/finite volume method. However, the fully-discretized model yields spurious high frequency oscillations which are often mistaken for density-wave oscillations due to discretization effects. One of the remedies for this problem is to use the moving boundary method to model the fluid flow in the heater tube. Unfortunately, a comprehensive review of literature indicates that this has not been done yet. To fill in this research gap, this paper

aims to propose a new low-order model using the moving boundary method to predict the low frequency PDO. This new model should not only eliminate the high frequency modes due to discretization artefacts, but also have the merits of preserving physical integrity with minimum dynamics states. The remainder of the paper is organized as follows. Section 2 describes the physical mechanisms of PDO. Section 3 gives the details of the proposed new model along with the conventional integral model and fully-discretized model. Simulation results are compared and discussed in Section 4. The conclusions are summarized in the final section.

2. MECHANISM OF PDO

Figure 1 illustrates the experimental system that is often used to study the PDO. The boundary conditions of the system, i.e., pressure p_i and fluid temperature T_i in the main tank as well as the exit pressure p_e, are kept constant. p is the pressure in the surge tank (compressible volume), while G_i and G_o is the mass flux entering and leaving the surge tank, respectively. Typical steady-state characteristic curves of pressure difference (between the surge tank and exit) versus G_i and G_o are also given. G_i curve (the external characteristics) is often a parabola that opens downward since it is plotted against p - p_e instead of p_i - p, whereas G_o curve (the internal characteristics) often exhibits an N-shape with two positive slope regions and one negative slope region. Under the steady-state operation, the equilibrium point can be determined by the following equations (Kakac and Bon, 2008)

$$p_i - p = K_i G_i^2 \tag{1}$$

$$p - p_e = f\left(G_{o,} Q\right) \tag{2}$$

$$G_i = G_o \tag{3}$$

where K_i and Q are the constant for the inlet restriction and heat input to the heater tube, respectively. The equilibrium is stable if it lies in the positive slope region of the internal characteristics. However, the equilibrium will be unstable if it is located in the negative slope region of the internal characteristics (as shown in Fig. 1). In this case PDO limit cycles will be likely to occur. When operating in the negative slope region, a slight increase in the surge tank pressure p will cause both G_i and G_o to decrease. Because the G_i curve is steeper than the G_o curve, G_o decreases more than G_i, resulting in more liquid accumulation in the surge tank and elevating its pressure p. Therefore, the operating point will move upward along the internal characteristics. When the operating point reaches its peak point A, there is still an imbalance between G_i and G_o, causing further increase in p. However, any higher surge tank pressure than point A is associated with a significant increase in G_i, which pushes system operation to the all-liquid side of the internal characteristics, i.e., point B. Since G_o is now much larger than G_i, p starts deceasing and then the operating point moves downward along the internal characteristics. When the operating point reaches the bottom point C, G_o is still larger than G_i, causing further decrease in p. Any lower surge tank pressure than point C is associated with a significant decease in G_i, which pushes system operation to the point D. Now G_i is less than G_o again, which causes the surge tank pressure to increase. As a result, the operating point moves upward until it reaches point A where another repeated PDO limit cycle starts again. In summary, as long as the equilibrium lies in the negative slope region of the internal characteristics, a small disturbance will push the system away from the equilibrium and result in limit cycles with trajectory *ABCDA*. Please note that the influence of system dynamics is not considered in the above qualitative analysis. Detailed analysis of limit cycle trajectory with system dynamics taken into account will be given in Section 4.

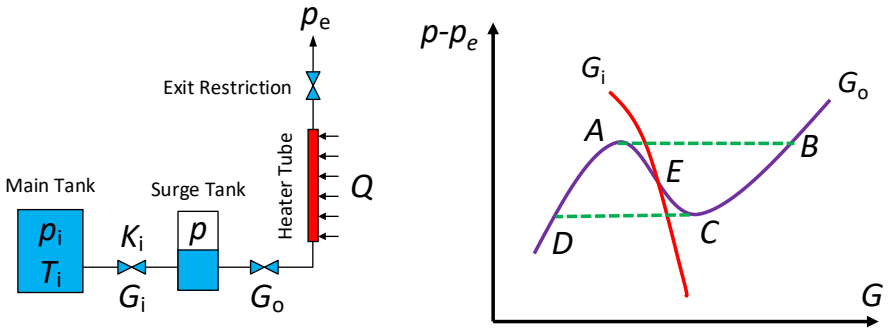

Fig 1. Schematic of the PDO system

3. THEORETICAL MODELS

In this section, we will describe the development of the proposed model using moving boundary method. Meanwhile, two conventional models (integral model and fully-discretized model) will be also presented to help readers better understand how these three models differ from each other in modeling the fluid flow in the heater tube. Before proceeding with that, the common assumptions of these models are given below.

(1) The main tank and the system exit maintain at constant pressures.
(2) Vapor phase and liquid phase are in thermodynamic equilibrium conditions
(3) Energy storage of heater tube walls is negligible.
(4) Pressure drop between the main and surge tank is concentrated at the inlet restriction.
(5) Pressure drop between the surge tank and system exit is concentrated in the heater tube.
(6) Two-phase homogeneous model.
(7) Local throttling losses between the surge tank and system exit are neglected.
(8) Heat input is uniformly supplied to the heater tube.

The inlet mass flux G_i can be determined by the momentum balance

$$\frac{dG_i}{dt} = \frac{1}{L_1}\left[\left(p_i - p\right) - K_i \frac{G_i|G_i|}{\rho_l}\right] \tag{4}$$

where L_1 is the pipe length between the main and surge tank.

The pressure dynamics in the surge tank can be described based on the mass balance (Stenning et al., 1967)

$$\frac{dp}{dt} = \frac{\left(G_i - G_o\right)A_c}{p_0 V_o \rho_l} p^2 \tag{5}$$

where p_0 and V_0 is the equilibrium pressure and the equilibrium volume of gas in the surge tank, respectively.

For the heater tube, one-dimensional momentum balance is considered.

$$\frac{\partial G}{\partial t} + \frac{\partial}{\partial z}\left(\frac{G^2}{\rho}\right) + \frac{\partial p}{\partial z} = -\rho g \sin\theta - \frac{f}{2D_h}\frac{G|G|}{\rho} \tag{6}$$

Please note that Eqs. (4) and (5) remain the same in all three models since the main difference between these models lies in the way how the heater tube is modeled. However, Eq. (6) will be handled differently in these models, which will be discussed in detail subsequently. For all models, p_i, p_e, K_i and Q are given, whereas G_i, G_o and p are the state variables that need to be computed.

3.1 Integral Model

Eq. (6) is a PDE that describes the temporal and spatial variations of fluid flow in the heater tube. In order to simplify the analysis, Eq. (6) will be integrated over the heater tube and a lumped model can be obtained with additional assumptions: (1) gravity effect is neglected, (2) mass flux G_o does not change spatially from the surge tank to system exit, and (3) linear enthalpy profile is assumed in the heater tube (Padki et al., 1992).

$$\frac{dG_o}{dt} = \frac{1}{L_t}\left[\left(p - p_e\right) - \frac{G_o^2}{\rho_l}\left(\frac{\rho_l}{\rho_e} - 1\right) - \Delta p_{fric}\left(G_o, Q\right)\right] \tag{7}$$

The enthalpy of fluid leaving the heater tube is

$$h_e = h_l + Q/\left(G_o A_c\right) \tag{8}$$

where h_l is the enthalpy of liquid entering the heater tube.

Comparing h_e with the enthalpy at the bubble and dew points h_f and h_g evaluated at the surge tank pressure p, it is very easy to determine whether the fluid flow exits the heater tube in the state of vapor, liquid or two-phase. Meanwhile, the length of respective regions (subcooled region, two-phase region, and superheated region) can be also calculated as follows.

$$L_{sc} = L_t\left[\min\left(h_e, h_f\right) - h_l\right]/\left(h_e - h_l\right) \tag{9}$$

$$L_{tp} = L_t\left\{\min\left[\max\left(h_e, h_f\right), h_g\right] - h_f\right\}/\left(h_e - h_l\right) \tag{10}$$

$$L_{sh} = L_t\left[\max\left(h_e, h_g\right) - h_g\right]/\left(h_e - h_l\right) \tag{11}$$

Different from the integral model in literature in which pressure drop is often calculated based on a curve-fitted function of mass flux and exit quality, this paper use Churchill correlation (Churchill, 1977) and Jung-Radermacher correlation (Jung and Radermacher, 1989) to calculate frictional pressure drop for single-phase and two-phase regions, respectively. Mean thermal-physical properties of fluid can be used to calculate pressure drop for single-phase region, while Newton-Cotes seven point formula can be used to numerically compute pressure drop for the entire two-phase region.

3.2 Discretized Model

It is evident that steady-state mass and energy balances are assumed in the integral model. However, these assumptions can be only justified for big compressible upstream tank and short heater tube. When the magnitude and the frequency of PDO increase, neglecting the inertia of mass and energy of two-phase flow can lead to significant errors when predicting its dynamics. Therefore, a discretized model is required to give more accurate results.

However, the standard model of a discretized pipe with n segments consist of 3n ODEs. In order to reduce model complexity, it is assumed that the time derivatives of pressures in the heater pipe is the same of that in the surge tank. With this assumptions, the number of ODEs reduces to 2n+1. The discretized equations using finite volume method for segment i are (Qiao et al., 2015; Qiao and Laughman, 2018).

$$\Delta z\left(\frac{\partial\rho_i}{\partial p_i}\frac{dp}{dt}+\frac{\partial\rho_i}{\partial h_i}\frac{dh_i}{dt}\right)=G_{i-1/2}-G_{i+1/2} \tag{12}$$

$$\Delta z\left(\rho_i\frac{dh_i}{dt}-\frac{dp}{dt}\right)=G_{i-1/2}\left(h_{i-1/2}-h_i\right)-G_{i+1/2}\left(h_{i+1/2}-h_i\right)+Q\Delta z/V_t \tag{13}$$

where the partial density derivatives are evaluated using the surge tank pressure.

The global momentum balance is given by

$$\frac{dG_o}{dt}=\frac{1}{L_t}\left[\left(p-p_e\right)-\left(\frac{G_{n+1/2}^2}{\rho_{n+1/2}}-\frac{G_o^2}{\rho_l}\right)-\sum_{i=1}^{n}\Delta p_{fric,i}\right] \tag{14}$$

In the above 2n+1 equations, there are n+1 state variables (p and h) and n algebraic variables (mass flux G). Please note that local frictional pressure drop will be evaluated for each segment and the total sum is used in Eq. (14).

3.3 Moving Boundary Model

The moving boundary method is characterized by dividing the pipe into different control volumes, each of which exactly encompasses a particular fluid phase (vapor, two-phase or liquid) and is separated by a moving boundary where fluid phase transition occurs. The one-dimensional governing equations are integrated over each control volume using the Leibniz integration rule. This method can significantly reduce model complexity while still preserving the prevailing physics. This paper uses the model presented in Qiao *et al*. (2016) and more details can be found in the paper. For the sake of brevity, here we only give the governing equations.

The mass and energy balances for the subcooled region are

$$L_{sc}\frac{d\overline{\rho}_1}{dt}+\left(\overline{\rho}_1-\rho_f\right)\frac{dL_{sc}}{dt}=G_o-G_{12} \tag{15}$$

$$L_{sc}\left(\overline{\rho}_1\frac{d\overline{h}_1}{dt}+\overline{h}_1\frac{d\overline{\rho}_1}{dt}-\frac{d\overline{p}_1}{dt}\right)+\left[\overline{\left(\rho h\right)}_1-\rho_f h_f\right]\frac{dL_{sc}}{dt}=G_o h_l-G_{12}h_f+\frac{L_{sc}}{L_t}Q \tag{16}$$

The mass and energy balances for the two-phase region are

$$L_{tp}\frac{\partial\overline{\rho}_2}{\partial\overline{p}_2}\frac{d\overline{p}_2}{dt}+\left(\rho_f-\rho_g\right)\frac{dL_{sc}}{dt}+\left(\overline{\rho}_2-\rho_g\right)\frac{dL_{tp}}{dt}=G_{12}-G_{23} \tag{17}$$

$$L_{tp}\left[\frac{\partial\overline{\left(\rho h\right)}_2}{\partial\overline{p}_2}-1\right]\frac{d\overline{p}_2}{dt}+\left(\rho_f h_f-\rho_g h_g\right)\frac{dL_{sc}}{dt}+\left[\overline{\left(\rho h\right)}_2-\rho_g h_g\right]\frac{dL_{tp}}{dt}=G_{12}h_f-G_{23}h_g+\frac{L_{tp}}{L_t}Q \tag{18}$$

The mass and energy balances for the superheated region are

$$L_{sh}\frac{d\overline{\rho}_3}{dt}-\left(\overline{\rho}_3-\rho_g\right)\frac{d\left(L_{sc}+L_{tp}\right)}{dt}=G_{23}-G_e \tag{19}$$

$$L_{sh}\left(\overline{\rho}_3\frac{d\overline{h}_3}{dt}+\overline{h}_3\frac{d\overline{\rho}_3}{dt}-\frac{d\overline{p}_3}{dt}\right)-\left[\overline{(\rho h)}_3-\rho_g h_g\right]\frac{d\left(L_{sc}+L_{tp}\right)}{dt}=G_{23}h_g-G_e h_e+\frac{L_{sh}}{L_t}Q \tag{20}$$

Please note that the model structure could change due to the varying number of fluid phases under large transients. In the context of PDO, the state of fluid leaving the heater tube could change periodically between vapor phase and two-phase. In this case, a numerically robust scheme is required to handle the switch between different model structures.

All three models were implemented in the Modelica language using the Dymola 2020x simulation environment, and the DASSL solver was used to integrate the set of differential algebraic equations with a tolerance of 10^{-5}.

4. RESULTS AND DISCUSSION

As the first step towards the comparison of these different models, we constructed three cases to verify the efficacy of these models. The conditions and parameters of these cases were given in Table 1. Figs. 2, 3 and 4 illustrated the simulation results for case 1, 2 and 3 with the integral model, discretized model and moving boundary model, respectively. It was evident that PDO with different amplitude and frequency was generated in each case, indicating that the models were appropriate. It was worth noting that the superimposed high-frequency mass flux oscillations observed in the results obtained by the discretized model were discretization artefacts and should not be mistaken for density-wave oscillations. These high-frequency oscillations were generated whenever the fluid state in a control volume transitioned between single-phase and two-phase, and the corresponding correlations for calculating pressure drop were switched. Since the discretized model did not track the phase boundaries, sudden change in pressure drop calculation could result in these discontinous edges. In comparison with the discretized model, the integral model and the moving boundary model did not exhibit these high-frequency modes because phase boundaries were tracked in these two models and the length of each phase was continous.

As mentioned earlier, the pressure-drop limit cycle shown in Fig. 1, which was often used to explain the generation mechanism of PDO, was nothing more than conceptual because it did not take system dynamics into account. Fig. 5 illustrated the stable trajectory of PDO in case 1 when system dynamcis were accounted for. The trajectory of the inlet mass flux G_i was counter-clockwise and intersected with the external characteristics at M and N. From Eq. (4), one can know that dG_i/dt should be equal to zero at both M and N, indicating that G_i would achieve its minimum and maximum at M and N respectively. When G_i was on the right-hand side of the external characteristics, it meant that G_i was larger than its corresponding steady-state value at the same surge tank pressure. As a result, dG_i/dt was negative and G_i would decrease accordingly, pushing the operating point to move upwad along the trajectory. Meanwhile, from Eq. (5) one can also know dp/dt will be positive when G_i was greater than the steady-state value, causing the surge tank pressure to increase. Therefore, both equations explained that G_i trajectory CNAMC moved in the counter-clockwise direction. In the contrast, the trajectory of the outlet mass flux G_o ABCDA moved in the clockwise direction. When G_o was above the internal characteristics, one can know that driving force p - p_e of G_o was greater than its required steady-state value that sustained the same mass flux. From Eq. (7) one can know that dG_o/dt should be positive and G_o will increase. On the other hand, when G_o was larger than G_i (G_o should be on the right of G_i), from Eq. (5) we can know that the surge tank pressure should decrease. Again, both Eq. (5) and (7) indicated that the G_o trajectory moved in the clockwise direction. G_o trajectory intersected with the internal characteristics at D and B where G_o achieved its minimum and maximum respectively because dG_o/dt was equal to zero at these two points. G_i and G_o trajectories intersected with each other at A and C where the surge tank pressure achieved its maximum and minimum respectively because G_i and G_o were equal and dp/dt was zero at these two points (see Eq (5)). Please note that the G_i and G_o trajectories did not intersect with the external characteristic at the same points, although in this case M and N were very close to A and C, respectively. The trajectories shown in Fig. 5 manifested that pressure drop limit cycle followed neither the internal nor external characteristics when system dynamics were present.

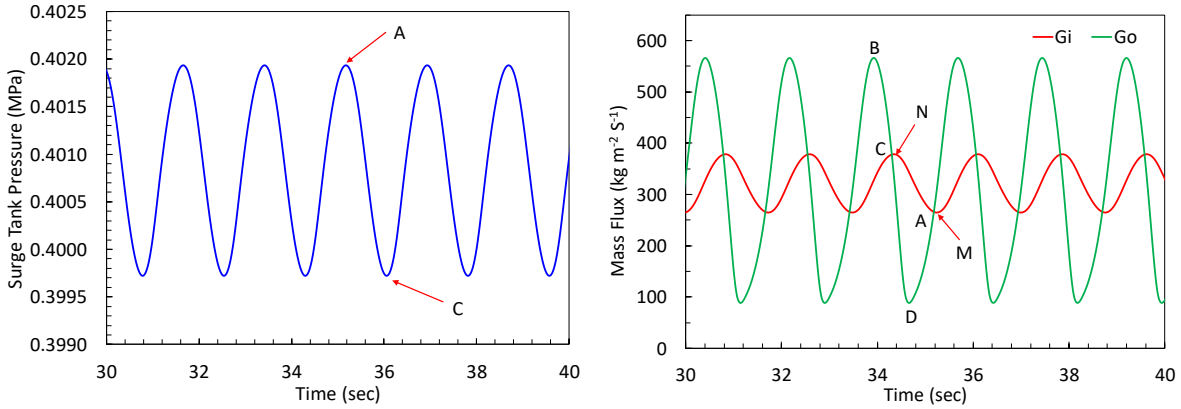

Fig. 2 PDO with the integral model (case 1): (a) surge tank pressure; (b) mass flux

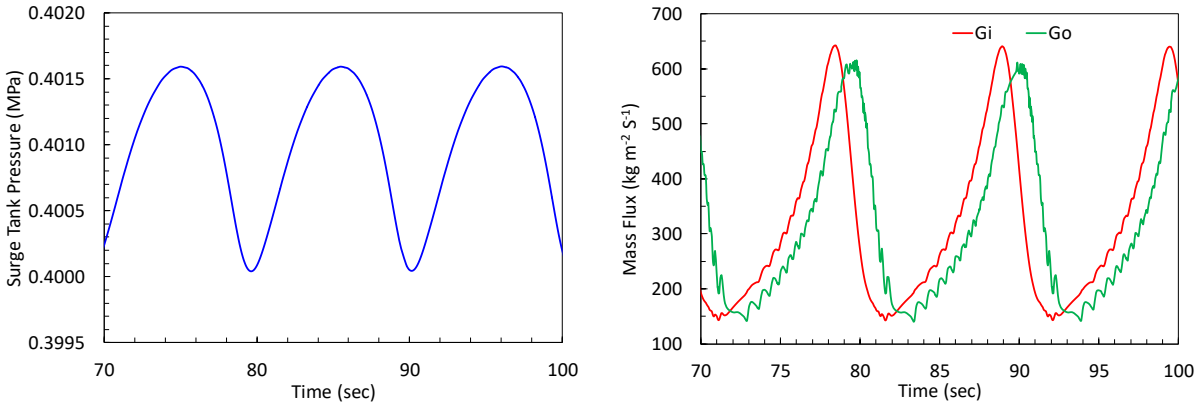

Fig. 3 PDO with the discretized model (case 2): (a) surge tank pressure; (b) mass flux

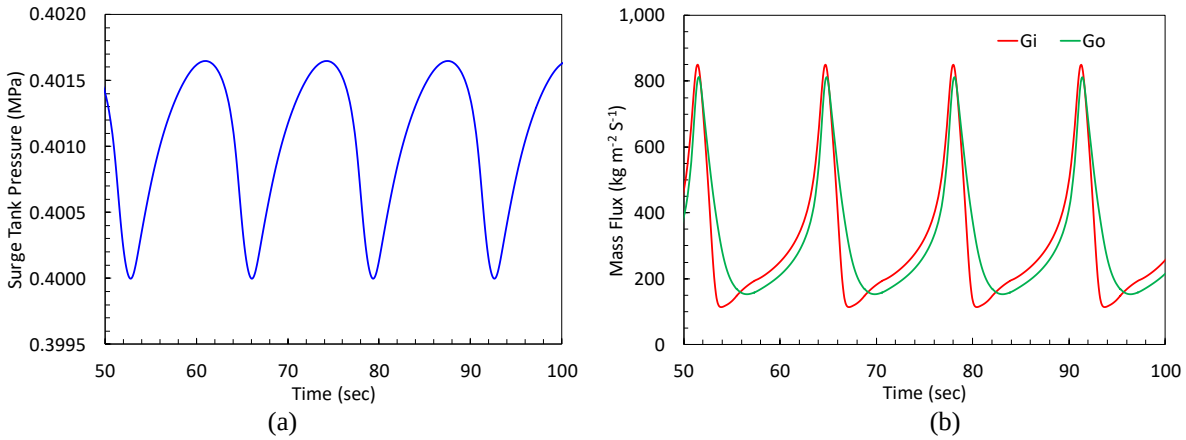

Fig. 4 PDO with the moving boundary model (case 3): (a) surge tank pressure; (b) mass flux

Table 1. Parameters of simulation cases

Parameter	Case 1	Case 2	Case 3
Fluid	R134a	R134a	R134a
Tube length (m)	1.2	0.6	0.6
Tube diameter (mm)	7	7	7
L_1 (m)	1.0	1.0	1.0
V_0 (liter)	0.7	5.0	7.0
K_i	40	40	40
Q (W)	850	1370	1500
p_i (Pa)	4e5+4e3	4e5+4e3	4e5+4e3
p_e (Pa)	4e5	4e5	4e5
T_i (K)	258	246	246
Single-phase DP	Churchill	Churchill	Churchill
Two-phase DP	Jung-Radermacher	Jung-Radermacher	Jung-Radermacher
Model	Integral	Disretized	Moving boundary

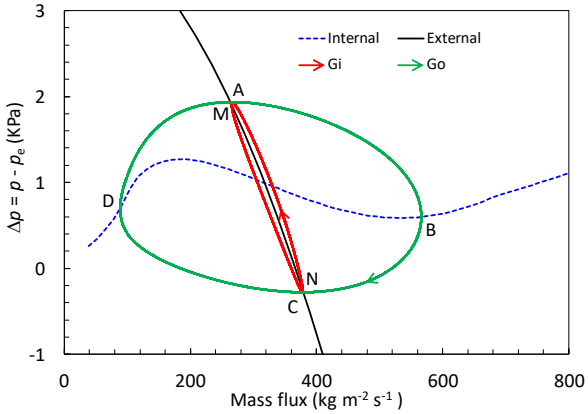

Fig. 5 Stable trajectory of pressure-drop limit cycle (case 1):
M, N - dG_i/dt = 0; B, D - dG_o/dt = 0; A, C - dp/dt = 0

The influence of heat input Q on the system instability was presented in Fig. 6. While the other parameters remained unchanged, there was a certain range of heat input that can produce pressure-drop limit cycles. As mentioned previously, one of the necessary conditions for PDO was that system equilibrium lied on the negative slope side of the internal characteristics. The shape of the internal characteristics changed when heat input increased, causing the system equilibrium to move along the external characteristics. The system was stable when there was no or little heat input, because the flow remained mostly liquid at this time and pressure drop across the heater tube increased monotonically with flow rate (e.g., the characteristic curves at 0W and 200 W), resulting an internal characteristics with positive slopes. When further increasing heat input, the internal characteristics started to exhibit an N-shape because frictional losses was proportional to the inverse of fluid density. However, the system was still stable because the equilibrium was on the positive slope side of the internal characteristics. When heat input continued increasing and exceeded the threshold, pressure drop oscillations occurred and the system became unstable because the stability conditions were not satisfied anymore. At this point, the equilibrium was on the negative slope side of the internal characteristics, as shown in Fig. 6b. As heat input further rose, the amplitude of oscillations increased before reaching the maximum. After that, the amplitude of oscillations started to decrease even with higher heat input. When heat input exceeded another threshold, the system became stable again because at this point the equilibrium was not on the negative slope side of the internal characteristics anymore (e.g., the characteristic curves at 1200W, 1400W and 1600W). Clearly, there were two bifurcation points where system stability can change when heat input varied and we will provide more analysis in the subsequent section.

The impact of inlet subcooling on system stability was shown in Fig. 7. Inlet subcooling is here defined as the difference between fluid temperature T_i and the corresponding saturation temperature at p_i. Similarly, there were also

two bifurcation points where system stability could change when fluid subcooling increased. At a given amount of heat input, pressure drop strictly increased with flow rate when there inlet subcooling was small. When inlet subcooling increased, the internal characteristics started to exhibit an N-shape because it was possible for fluid to leave the heater tube in either two-phase or liquid state, depending on the amount of flow rate. When inlet subcooling rose above the low threshold, pressure drop oscillations occurred and the amplitude of oscillations increased. When inlet subcooling was greater than the high threshold, oscillations disappeared and the system became stable again because the equilibrium moved to the positive slope side of the internal characteristics. Meanwhile, it was observed that inlet subcooling had not exerted substantial influence on the frequency of oscillations, which decreased marginally when increasing inlet subcooling.

The effect of the equilibrium volume of gas V_0 in the surge tank on system stability was illustrated in Fig. 8. It was evident that there was a minimum compressible volume required to produce pressure drop limit cycles for a given system. When the compressible volume was greater than the threshold, the amplitude and frequency of oscillations both grew rapidly to the peaks and then decreased gradually with increasing the compressible volume.

The direct comparison of all three models under the same operating conditions of case 1 was given in Fig. 9. It was shown that the integral model predicted oscillatory behavior, whereas the other two models predicted a stable operating point. This interesting finding indicated that the dynamic behavior of fluid flow in the heater tube had to be taken into account and unexpected results could be attained. However, this statement did not imply that the integral model should be abandoned and it had its advantages in stability analysis because of simplicity, which will be shown in the next section.

Eigenvalues of three models at the operating conditions in case 1 were plotted in Fig. 10. For the integral model, there were two eigenvalues on the right-hand side of the complex plane, indicating that the system was unstable. For the other two models, all eigenvalues were on the left-hand side of the complex plane, indicating that the system was stable. This comparison manifested the differences between these three models, and once again was consistent with the simulation results shown in Fig. 9.

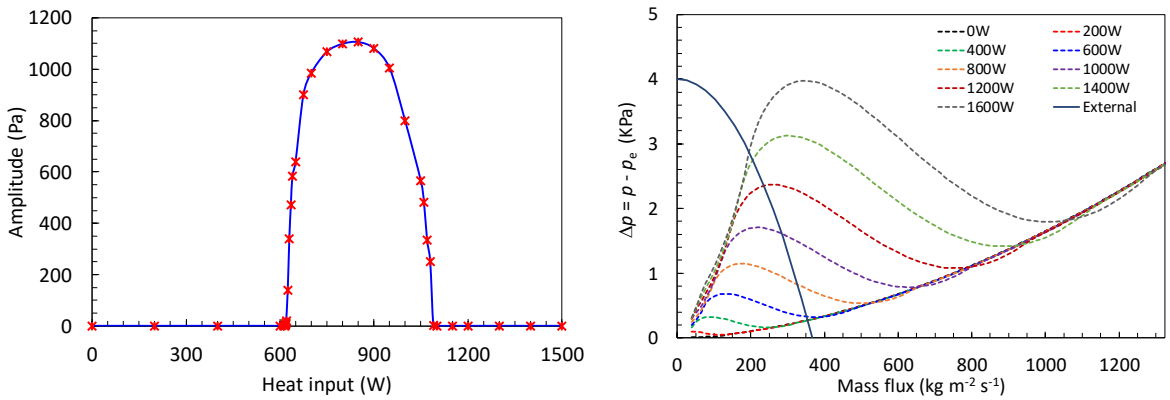

Fig. 6 Effect of heat input on system stability (case 1):
(a) PDO amplitude vs. heat input; (b) Δp-G_o curves at different heat input

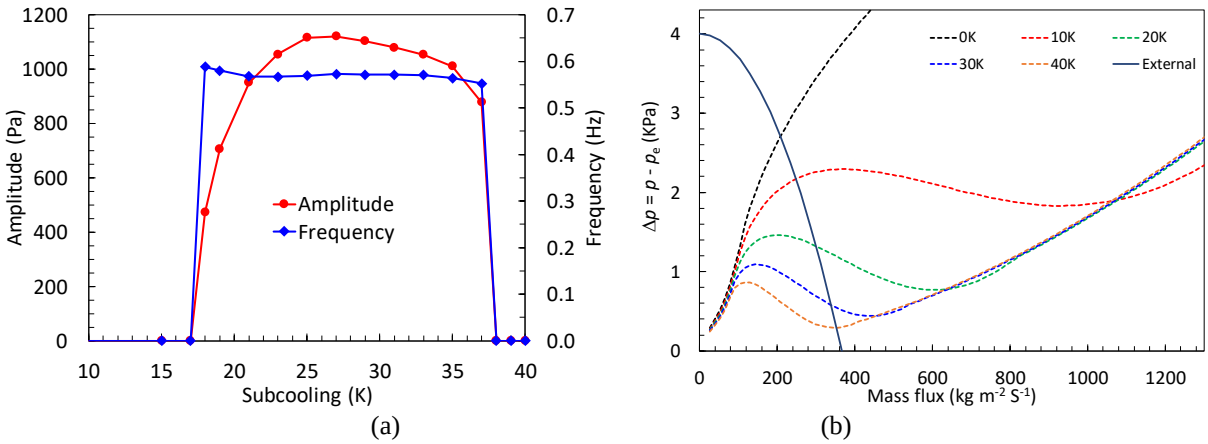

Fig. 7 Effect of inlet subcooling on system instability (case 3):
(a) PDO amplitude and frequency vs. subcooling; (b) Δp-G_o curves at different subcooling

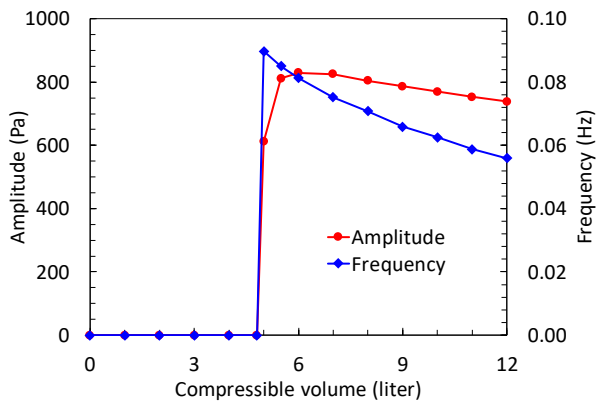

Fig. 8 Effect of V_0 on system instability (case 3)

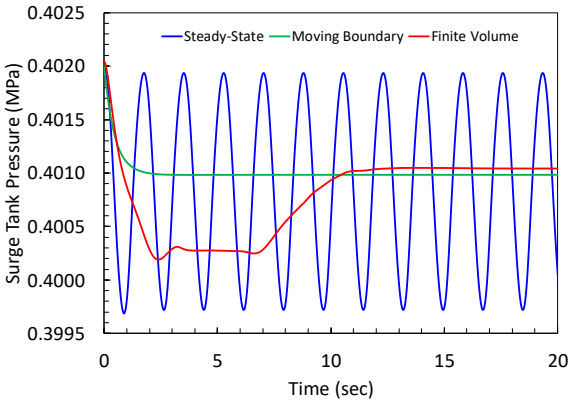

Fig. 9 Comparison of model results

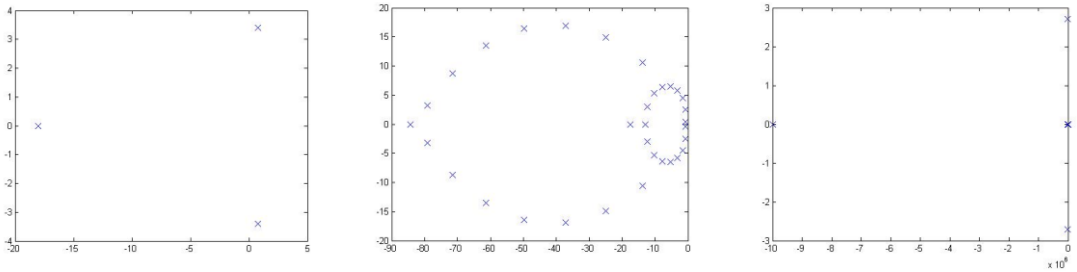

(a) (b) (c)

Fig. 10 Eigenvalues of three models (case 1):
(a) Integral model; (b) Discretized model; (c) Moving boundary model

5. CONCLUDING REMARKS

We have presented three different models to successfully simulate pressure drop oscillations. The advantages and disadvantages of these models were discussed. Simulation studies were carried out to explore the effect of various parameters on system stability. It was demonstrated that these models can provide valuable insight into the

mechanisms that generate pressure drop oscillations. Observations in the root locus analysis were consistent with the simulation results.

NOMENCLATURE

Symbols		***Subscripts***	
A_c	cross sectional area	e	exit of heater tube
D_h	hydraulic diameter	f	saturated liquid
f	frictional factor	g	saturated vapor
g	gravity constant	i	inlet or segment index
G	mass flux	n	number of segments
h	specific enthalpy	o	outlet
K_i	inlet restriction coefficient	sc	subcooled
L	length	sh	superheated
p	pressure	tp	two-phase
Q	heat flow rate		
t	time		
V	volume		
Δ	difference		
ρ	density		

REFERENCES

Churchill, S.W., 1977. Frictional equation spans all fluid flow regimes. *Chem. Eng.* 84, 91-92.

Jung, D.S. and Radermacher, R., 1989. Prediction of pressure drop during horizontal annular flow boiling of pure and mixed refrigerants. *Int. J. Heat Mass Transfer* 32 (12), 2435-2446.

Kabac, S. and Bon, B., 2008. A review of two-phase flow dynamic instabilities in tube boiling system. *Int. J. Heat Mass Transfer* 51, 399-433.

Qiao, H., Aute, V., Radermacher, R., 2015. Transient modeling of a flash tank vapor injection heat pump system - Part I: Model development. *Int. J. Refrigeration* 49, 169-182.

Qiao, H., Laughman, C.R., Aute, V., Radermacher, R., 2016. An advanced switching moving boundary heat exchanger model with pressure drop. *Int. J. Refrigeration* 65, 154-171.

Qiao, H. and Laughman, C.R., 2018. Comparison of approximate momentum equations in dynamic models of vapor compression systems. *16th International Heat Transfer Conference*, Beijing, China.

Ruspini, L.C., Marcel, C.P., Clausse, A., 2014. Two-phase flow instabilities: A review. *Int. J. Heat Mass Transfer* 71, 521-548.

Stenning, A.H., Veziroğlu, T.N., Callahan, G.M., 1967. Pressure-drop oscillations in forced convection with boiling system. *Proc. Symp. on Dynamics of Two-phase Flows*, EUROTOM.